Received: 16 September 2020 | Revised: 18 December 2020 | Accepted: 18 December 2020

DOI: 10.1002/pls2.10026

RESEARCH ARTICLE

SPE INSPIRING PLASTICS PROFESSIONALS SPE POLYMERS WILEY

Experimental investigations on process parameters for manufacturing of antenna reflectors using vacuum infusion process

Tushar Gajjar | **Dhaval B. Shah** | **Shashikant J. Joshi** | **Kaushik M. Patel**

Mechanical Engineering Department, Institute of Technology, Nirma University, Ahmedabad, India

Correspondence
Tushar Gajjar and Dhaval B. Shah, Mechanical Engineering Department, Institute of Technology, Nirma University, Ahmedabad 382 481, India.
Email: tushar.gajjar79@gmail.com (T. G.) and dbshah@nirmauni.ac.in (D. B. S.)

Abstract

Carbon fiber reinforcement polymers (CFRPs) are commonly used in aerospace, automobile, and sports industries due to its superior properties compared to conventional metal and alloys. Vacuum infusion process (VIP) is one of the more versatile open mold composite manufacturing techniques because of its economic viability. This paper describes the fabrication of CFRP antenna reflectors used in space communication applications using VIP. Number of layers and pressure gradient were considered as process parameters to evaluate dimensional accuracy. Non-contact 3D scanning has been used to measure the deviation from fabricated reflector and theoretical CAD model of reflector. Subsequent spring-back deformation has also been obtained for each reflector. Part thickness at various locations along the length has been measured, whereas the fiber volume fraction has been calculated for each reflector. ANSYS Fluent software has been utilized to acquire pressure drop throughout the reflector, and the calculated pressure drop was validated by relating compaction pressure and volume fraction. The mold filling time has also been measured during the manufacturing process for different laminate thicknesses.

KEYWORDS

antenna reflector, dimensional accuracy, pressure variation, vacuum infusion process, volume fraction

1 | INTRODUCTION

A composite material is the combination of two or more materials at the macroscopic level and is often done to give high strength. The manufacturing process plays a vital role in determining the final properties. There are many manufacturing processes for composites, viz. hand layup process, autoclave process, VIP process, resin transfer molding (RTM) process, etc. The VIP process, one type of liquid compaction molding (LCM) process, has been widely used over many decades to manufacture composite material because of the advantages of room temperature processing, cost-effectiveness, and easy availability.[1] VIP process usually consists of one mold on the bottom and the top covered with a vacuum bag. This process is cheaper than RTM or autoclave processes.[2] Broadly, fibers used in composite materials are classified as natural and manmade fibers. Manmade fibers have superior properties compared to natural fibers, with carbon fibers having higher specific strength

This is an open access article under the terms of the Creative Commons Attribution License, which permits use, distribution and reproduction in any medium, provided the original work is properly cited.
© 2020 The Authors. *SPE Polymers* published by Wiley Periodicals LLC. on behalf of Society of Plastics Engineers.

and specific stiffness. Carbon fiber reinforced polymers (CFRPs) find widespread applications in aerospace, automobile, sports, defense, and space applications. Sixty to seventy percent of space components have been manufactured using CFRP materials.[3] A parabolic antenna reflector is one of the components used in space communication applications and must have high dimensional accuracy. Many researchers have worked on the minimization of spring-back deformation by various methods, including manufacturing techniques.

In VIP process, the formation of voids during the mold filling stage for complex geometry is unavoidable. Void formation can be eliminated through active control schemes and enhancement of flow in VIP process using localized induction heating.[4–6] The equivalent permeability method was used to reduce computational time for VIP flow simulation of large parts.[7] The finite element model was developed to analyze a fiber preform infiltration with resin under non-isothermal conditions during the VIP process.[8] Similarly, injection design methodology was illustrated for low permeability preforms and the thick section using inter-laminar flow media.[9] The void distribution is significant for manufacturing a large component and depends on the gap distance between fiber tows as well as the individual gap distance between fiber strands.[10] The thickness of the manufactured part in VIP processes changes with resin inlet geometry.[11,12] The flow rate was controlled using a piston-based injector system in VIP technique.[13,14] The resin flow rate will be affected by the permeability of the medium as well as resin inlet size and geometry. Moreover, resin flow also changes with the contour of the mold surface.[15] Dai et al.[16] investigated different VIP techniques in manufacturing cost and time for the sandwich panels. Jeffrey et al.[17] simulated resin flow in the VIP process using the control volume method. This author developed a numerical model for resin flow thorough out the fiber tow. Markicevic et al.[18] studied a preform quality and variation in distribution media permeability.

Large-sized complex shape components, mostly used in space applications, are difficult to manufacture with proper dimensions. The spring-back deformation depends on many process parameters like manufacturing methods, demoulding process of manufactured component, curing time, and properties between fiber and epoxy. Shah et al.[19] manufactured antenna reflectors using an autoclave process by selecting various process parameters like mold materials, layup orientation, number of layers, and curing cycle. Gajjar et al.[20] studied spring-in deformation of L-shaped CFRP components using experimental and simulation approaches for unidirectional, cross-layups, quasi-isotropic laminate orientation, including the various number of layers. Kim et al.[21] used the brake forming process for determining spring-back deformation for L-shaped metal matrix composite. Moreover, the pressure variation and flow progression were also studied for VIP process. The sensitive pressure transducer was used for obtaining pressure values along the length.[22–26] The part thickness variation and pressure gradient were studied by considering various resin inlet positions, dry and wet forms of fabric of the material.[27–29]

Many researchers worked on various process parameters for the quality of the composite product manufactured using the VIP. The effect of permeability, fiber volume fraction, thickness of laminate, pressure distribution, resin flow intensity, curing cycle, fiber orientation, etc., were significant process parameters in VIP, which decides the near-net-shape the product. The resin flow in the mold was simulated based on the resin inlet position using numerical modeling by few researchers. Very few studies were devoted to the effect of different process parameters on dimensional accuracy for complex shape components. High dimensional conformity is the principal challenge for CFRP antenna reflector used in space communication applications.

In this research paper, the VIP process was used for manufacturing CFRP antenna reflectors. Non-contact 3D scanning technique was used to measure the deviation at the inner surface of the reflector with 200 locations. Spring-back deformations for 4, 8, and 12 layer components were calculated. The part thickness was measured at different locations of manufactured reflectors. The effect of part thickness and fiber volume fraction with respect to different locations was studied along with compaction pressure. The pressure variation was simulated in ANSYS Fluent, and the results were validated with an analytical approach. The mold filling time was measured for 4, 8, and 12 layer antenna reflectors.

2 | EXPERIMENTATION

2.1 | Material selection

AISI 430 grade was used as the mold material because of ease of accessibility and good thermo-mechanical properties. The bi-axial carbon fiber supplied by the Formosa Plastic Corporation was used as a reinforcement material. Resin 520 was used as the epoxy mixed with hardener D at a 70:30 ratio. Specifications of these materials are shown in Table 1. Other consolidated materials, like release agent, peel-ply, purported plastic, vacuum bag, release tape, catch pot were procured to perform the VIP process.

TABLE 1 Specification of materials

Carbon fiber	**Tensile strength (MPa)** **areal weight (g/m^2)** **tensile modulus (GPa)**	**4000** **200** **230**
Epoxy Resin 520	mix viscosity at 27°C (MPas)	650 ± 100
	specific gravity (g/cm^3)	1.15–1.18
	pot life at 27°C (hrs)	1.5–2
D-type hardener	tensile strength (MPa)	70
	flexural strength (MPa)	120
	impact strength (N/m)	80

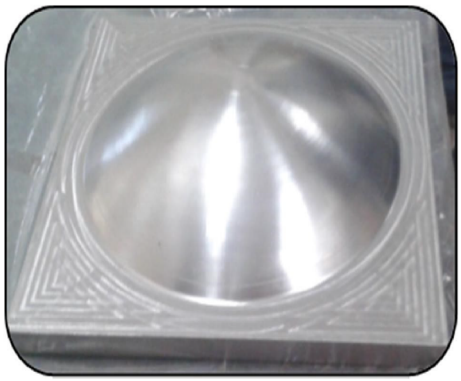


FIGURE 1 Manufactured mold after machining

2.2 | Experimental process

The metallic block of size, 300 mm × 300 mm × 70 mm was purchased as the mold. The parabolic profile had a 50 mm depth with 240 mm circumferential diameter. The mold dimension was based on the scaled size of standard antenna reflector sizes used in space applications. The entire mold was machined by implementing NC coding in 5-axis vertical machining center. The machined mold with a good surface finish is shown in Figure 1. Three to four layers of release agent were applied on the mold surface to ease the demoulding process. Number of layers for bi-axial dry carbon fabric was mounted sequentially. All layers of fabric were oriented in the same direction, that is, at $[0^\circ]_s$or unidirectional for the 4, 8, and 12 layer laminates. Results were compared in terms of dimension accuracy, part thickness variation, mold filling time, volume fraction along the length. The line diagram for the experimental setup, including mold, carbon fabric, and other consolidated materials, is shown in Figure 2.

The circular layer of peel ply and two layers of breather cloth of the same size were placed on top of the carbon fiber fabric. Sealant tape was applied at the boundary of the mold to make a leak-proof assembly. The layer of purported plastic and subsequent layers of infusion mesh was kept on the peel ply. The entire setup was vacuum bagged using a vacuum film and valve. PVC hose pipe has been connected with a resin inlet at one end and vacuum pump on the other side. Leakage was checked for 5–10 min by generating the vacuum inside the assembly. The inlet valve was opened after confirming an airtight setup, and at the same time, vacuum was applied to suck the resin through the PVC pipe and slowly through the carbon fabric layers, as demonstrated in Figure 3(A). The vacuum pressure was applied continuously for 24 h to obtain a high-quality product.

The resin flow continues once the filling stage is over and takes a finite time to achieve constant pressure during the post-filling period. The pressure inside the mold is continuously changing during the post-filling stage, which depends on resin inlet condition.[30] The post-filling stage allows resin pressure to equilibrate within the cavity and contains the removal of excess resin. The pressure at the inlet remains higher than at the outlet. So, the thickness gradient in the laminate changes during the post-filling stage.

The entire assembly was put in a hot air oven at 80°C for 4 h to get high bonding between carbon fabric and epoxy resin system. The final reflector was demoulded from the stainless steel mold and is shown in Figure 3(B).

3 | RESULTS AND DISCUSSIONS

3.1 | Measurement of dimensional accuracy for reflectors using 3D scanning

Developer spray was applied on the manufactured reflectors' inner surface to highlight the black surface. The black and white stickers were randomly placed on the surface to obtain reference points. A high precision 3D scanner was used to measure specified coordinate points on the internal surface of the reflectors. The scanned surface was generated based on the marked reference points and point cloud data obtained by the compatible software. This generated surface was superimposed with the original CAD surface. The deviation at a predefined point was acquired by comparing the scanned surface with the actual CAD model.

The internal surface of the reflector was divided into 200 coordinate points to measure the deviation between the theoretical CAD model and fabricated reflector. These 200 coordinate points were obtained at nine-degree rotations from the top surface, and five points were taken

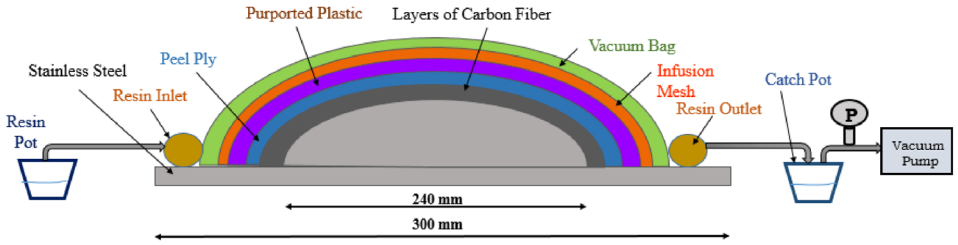


FIGURE 2 Line diagram of VIP process. VIP, Vacuum infusion process

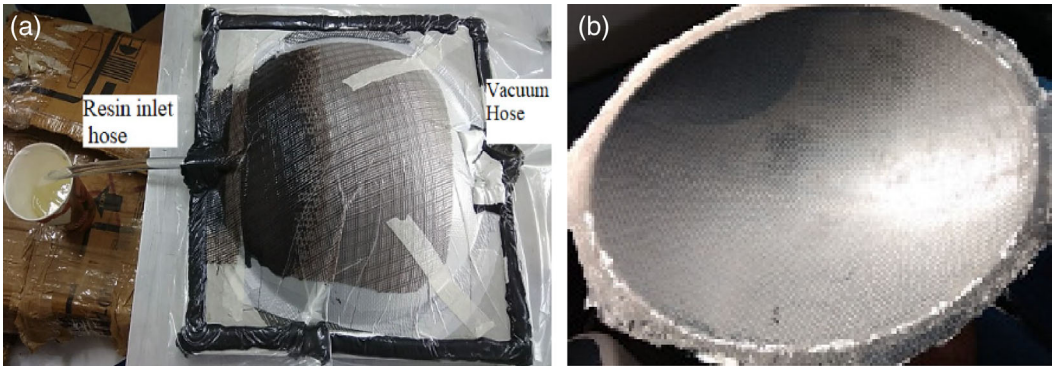


FIGURE 3 (A) Experimental setup during resin flow (B) manufactured reflector

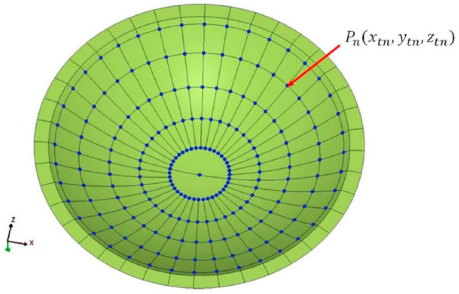


FIGURE 4 The CAD model of parabolic reflector with theoretical (x_t, y_t, z_t) coordinates[19]

at one line, as shown in Figure 4, with the result shown in Figure 5. The deviation of the scanned reflector was higher at the curvature surface outer edge and lower near the center point. This deviation was observed along all axes of the reflector.

The deviation of the entire reflector was calculated using Equation (1).

Deviation:

$$d_n = \sqrt{(a_{na} - a_{n1})^2 + (b_{na} - b_{n1})^2 + (c_{na} - c_{n1})^2}, \quad n = 1, 2, \ldots, 200. \tag{1}$$

Where a_a, b_a, c_a are measured x, y, and z coordinates using 3D scanner and a_1, b_1, c_1 are theoretical x, y, and z coordinates of the 3D CAD model. The deviation of the component at each point was taken as d. The total

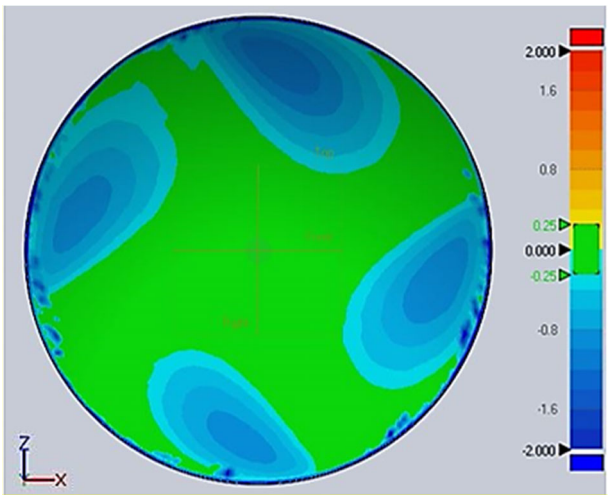


FIGURE 5 Deviation of manufactured reflector after scanning 200 coordinate points

deviation, which is referred to as spring-back deformation of manufactured reflector, was calculated based on deviation at each point. The root mean square (RMS) difference was calculated using Equation (2).

$$\varepsilon_{rms} = d_{rms} = \sqrt{\frac{1}{n}({d_1}^2 + {d_2}^2 + \ldots\ldots + {d_n}^2)}, \quad n = 200. \tag{2}$$

where ε_{rms} is the spring-back deformation value. The average spring-back defamation for 4, 8, and 12 layers of manufactured antenna reflector was measured as

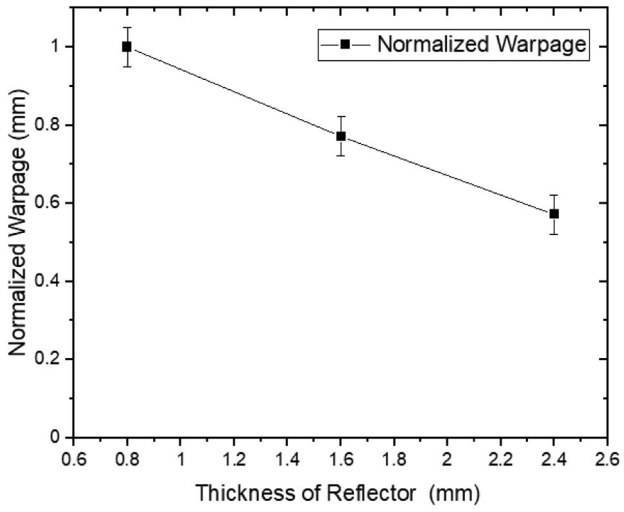


FIGURE 6 Normalized warpage for different thicknesses antenna reflectors

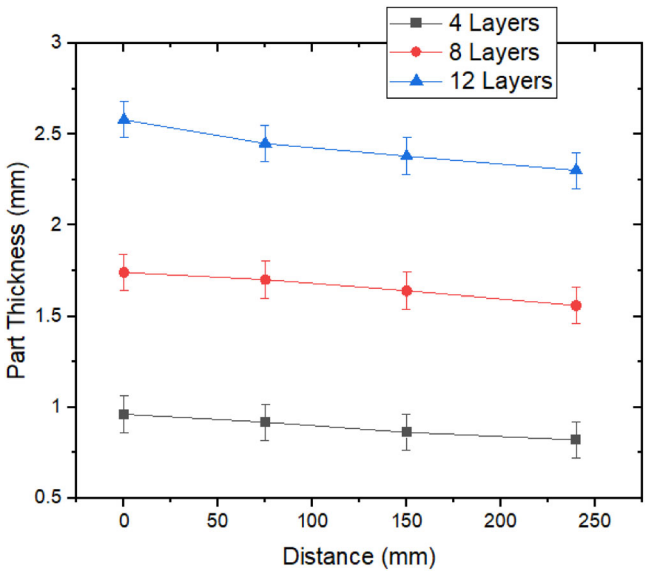


FIGURE 7 The part thickness variation with respect to distance for antenna reflectors with different thickness

0.35 mm, 0.27 mm, and 0.20 mm. The warpage for all reflector thicknesses was collapsed onto a single plot by normalizing the warpage for any thickness reflector to the warpage for a four layer reflector. The variation in normalized warpage for the different number of layers of antenna reflectors is shown in Figure 6. Again, the warpage decreased with increasing the number of layers. Thin components have more significant warpage than thick components because the same deviation in laminate thickness affects the measured warpage more for a thinner component.[19] The average normalized warpage is inversely proportional to the thickness of the components.

3.2 | Measurement of part thickness and fiber volume fraction for manufactured reflectors along the length

The thickness for a single layer of carbon fabric was 0.2 mm; therefore, the maximum thickness for the 4, 8, and 12 layers antenna reflectors are 0.8, 1.6, and 2.4 mm, respectively. The thickness was measured at the resin inlet position, 80 mm, 160 mm, and at the resin outlet position along the total 240 mm longitudinal total length of the reflector. The variation in part thickness along the resin flow direction, considering the average value across the transverse direction of the flow, is plotted in Figure 7. The thickness variation of different laminates varied between 5%–10% with respect to theoretical thickness. The average thickness of antenna reflectors along the resin flow direction decreased from the resin inlet to outlet position because of the resin pressure difference across the length. Experiments conducted by Acheson et al.[17] also confirm this phenomenon. The part thickness for the component is inversely proportional to the fiber volume fraction in this process. The fiber volume fraction behavior and the part thickness variation with an increasing number of layers in composite laminate are in accordance with the literature.[26,31]

The maximum fiber volume fraction was achieved in the VIP compared to other open mold processing of polymer composite like hand layup, spray layup, etc. techniques. The fiber volume fraction across the length of the reflector is calculated using Equation (3), which depends on the thickness of the component. The fiber volume fraction varies between 40%–60% and increased with distance from the inlet, as shown in Figure 8, again because of the decrease in fluid pressure along the infusion length. These results agree with experiments conducted by Vila et al.[26] and Yuexin et al.[32] The resin pressure is responsible for the compaction of the reinforcement and directly affects the final fiber volume fraction of the part.[33] The presence of the void in dry conditions will accelerate the impregnation and lubrication phase for thick laminates, which results in a higher initial fiber volume fraction.

$$V_f = \frac{\rho_{Sup.f}}{\rho_{fiber}} \times \frac{1}{h} \times n. \quad (3)$$

where V_f = fiber volume fraction, n = total number of layers, $\rho_{Sup.\ f}$ = superficial density or area density of fiber, ρ_{fiber}= fiber density and h = thickness of the laminate.

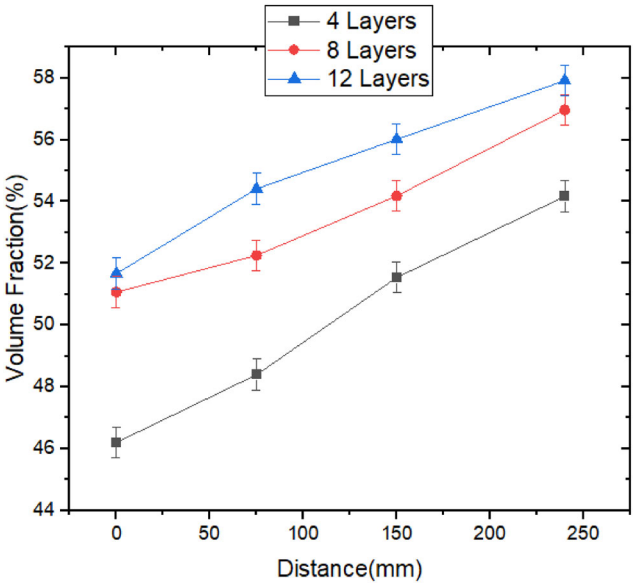


FIGURE 8 Fiber volume fraction variation with respect to distance for antenna reflectors with different thickness

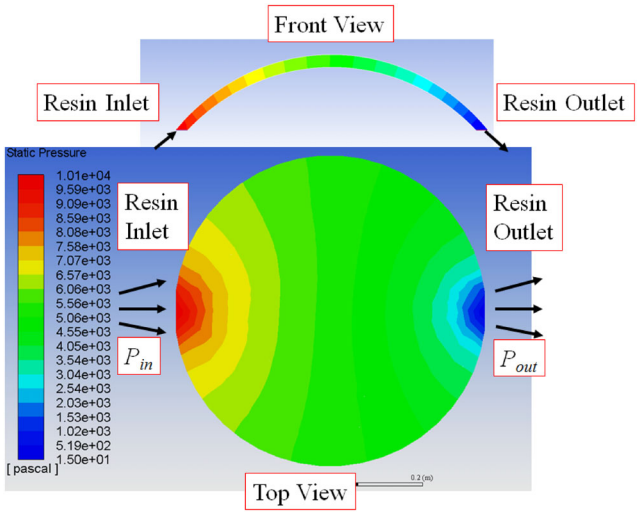


FIGURE 9 The static pressure distribution of four layer antenna reflector

The compaction behavior of fiber-reinforced polymer composites plays a crucial role in the composite manufacturing process. The compaction pressure and thickness reduction are in a linear relationship above a specific pressure. The thickness variation depends on the position of resin inlet in composite components. Higher local fluid pressure at the resin inlet reduces compaction pressure and increases thickness. The compaction pressure is minimum at the resin inlet position and maximum at the resin outlet. Our results are in good agreement with results obtained by Yenilmez et al.[29] and Correia et al.[34]

3.3 | Prediction of pressure variation of antenna reflector using a simulation approach

The pressure at any point in the mold is divided into resin pressure (P_r) and compaction pressure (P_c) in VIP. The atmospheric pressure (P_{atm}) is only considered as there is no external pressure applied in this process. The relation of atmospheric pressure with resin pressure and compaction pressure is given in Equation (4).

$$P_{atm} = P_r + P_c. \tag{4}$$

$$\therefore \quad P_c = P_{atm} - P_r. \tag{5}$$

The pressure ($P(x)$) for antenna reflector in one-dimensional linear flow is written as Equation (6).

TABLE 2 The fiber volume fraction and stiffing index for different laminate

Number of layers	V_{fo}	B
4	36.2312	0.0826
8	32.2668	0.0373
12	37.1234	0.04672

$$P(x) = P_r + \frac{P_v - P_r}{L}x. \tag{6}$$

Where L is the component length, $P_v$is the vacuum pressure, and x is variable at a linear distance ($0 < x < L$). Further,

$$\text{At } x = 0, P(0) = P_r = P_{atm}.$$

$$\text{At } x = L, P(L) = P_v.$$

The pressure distribution across the antenna reflector was simulated as flow through porous media using ANSYS Fluent software. The antenna reflector's CAD geometry was prepared using solid modeling software and subsequently imported into the software. Some portions of the geometry were considered as frozen, while the remaining was considered as porous media. The entire geometry was meshed with an element size as per the accuracy requirement. The resin pressure at inlet and outlet has been considered as atmospheric and vacuum pressure, respectively. In addition, the other required properties like resin density, velocity of resin, average permeability, the thickness of cloths were used during the analysis.[35] The porous jump value was calculated using the dimension and properties of the reflector.[36]

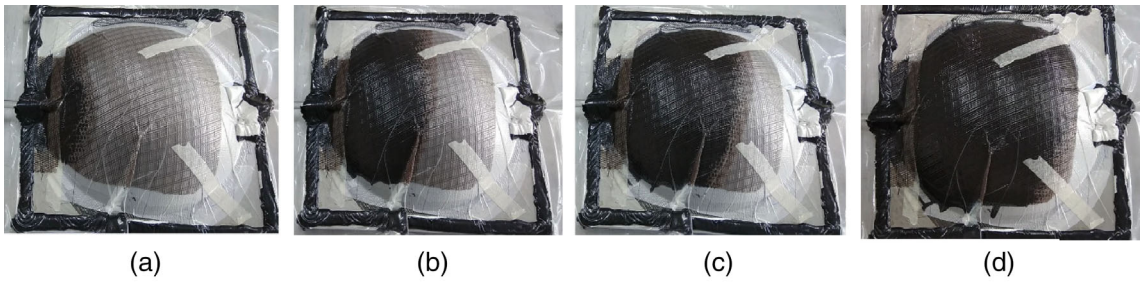


FIGURE 10 The resin flow with covering (A) 1/4, (B) 1/2, (C) 3/4, and (D) full area of the antenna reflector

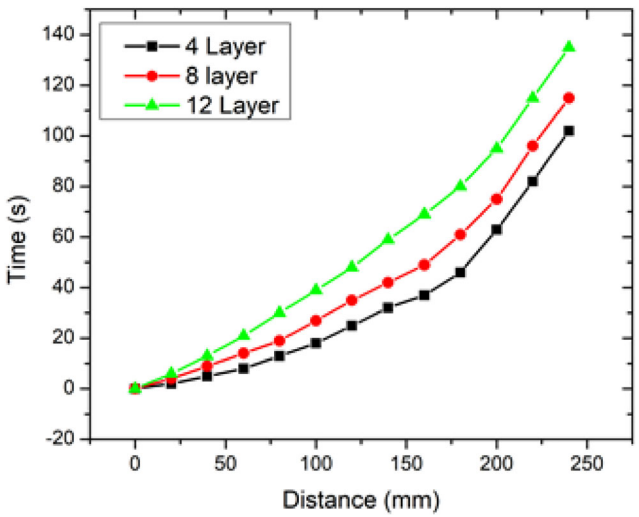


FIGURE 11 The mold filling time with respect to distance for antenna reflectors with different thickness

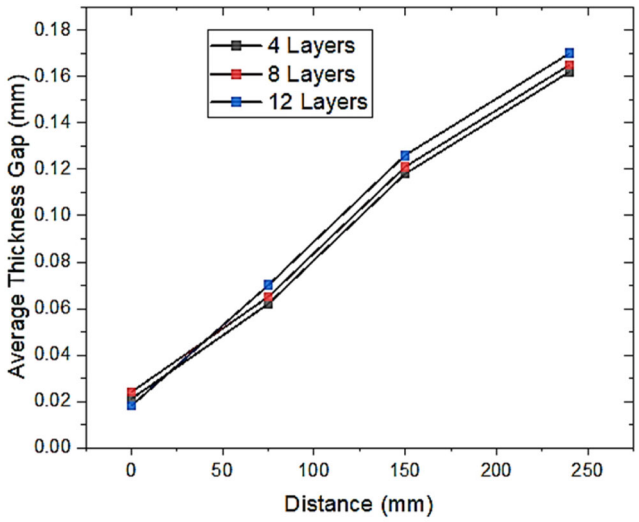


FIGURE 12 Average thickness variation of reflector along the length of the antenna reflectors

The variation of resin pressure at different locations was obtained as an output of simulation results. Static pressure distributions from simulation results for four layers reflector are shown in Figure 9. The static pressure decreases with increasing distance from the inlet along the length of the component. Figure 9 shows that the resin first covers the center area and then moves to the corners. The relation between fiber volume fraction and compaction pressure is given in Equation (7).

$$V_f = V_{f0} \times \left(P_{comp}\right)^B. \quad (7)$$

V_{f0} is the fiber volume fraction at 1 Pa pressure, and B is a stiffing index which is controlled fiber structure and varies between 0 to 1. The value of V_{f0} and B were calculated based on obtained pressure at different locations and verified with the experimental results conducted by other researchers. The value of the compaction pressure was calculated according to Equation (5), and the fiber volume fraction was taken from the measured part thickness values with respect to distance, according to Equation (3). Based on compaction pressure and fiber volume fraction, the value of V_{f0} and B were calculated for 4, 8, and 12 layer laminates, as shown in Table 2, and was also validated with the compaction model data described by Correia et al.[34]

3.4 | Measurement of mold filling time for manufacturing antenna reflector

The mold filling time was measured visually for each antenna reflector. The purpose of the infusion mesh in the vacuum infusion process is to transfer resin uniformly in all directions and at high speed in selected areas. The permeability of the infusion mesh and the carbon fabric are different. The infusion mesh was placed at the top surface of the other consolidation materials and then covered with a vacuum bag. The resin passes through the infusion mesh first and then from the top layer to the bottom layer of the carbon fiber cloths. Flow fronts shown in Figure 10 indicate the resin position in the infusion mesh at fixed equal time intervals. Simultaneously, the flow fronts through different carbon fabric layers are lagging compared to top infusion

mesh because of the high porosity. Mold filling times along the longitudinal direction for 4, 8, and 12 layers laminate have been shown in Figure 11.

3.5 | The average thickness variation along the length of the components

The thickness variation (Δh) before and after curing along the length has been determined via Equation (8) for each reflector and is shown in Figure 12.

$$\Delta h = |h - h_1|. \tag{8}$$

where h = initial part thickness of the components before curing, h_1 = final part thickness of the components after curing. Plotted values in Figure 12 are an average thickness variation along the length of antenna reflectors.

4 | CONCLUSIONS

The spring-back deformation, compaction pressure, part thickness, fiber volume fraction, pressure variation, and mold filling time were acquired for each CFRP parabolic antenna reflector fabricated using VIP. The maximum spring-back deformation was found for 4 layers, whereas a minimum was found for 12 layer reflectors. Warpage variation in 8 and 12 layer reflectors is 33% and 42% less than four layers reflectors. Thin components have more significant warpage because the same deviation in laminate thickness affects the measured warpage more for a thinner component. The average thickness of the antenna reflectors along the resin flow direction decreased from the resin inlet to the resin outlet position due to the difference in resin pressure during the manufacturing process. The fiber volume fraction was higher for thick laminates compared to thin laminates. The resin pressure is responsible for the compaction of the reinforcement and directly affects the final fiber volume fraction of the part. The pressure distribution across the antenna reflector was simulated as a flow through porous media using ANSYS Fluent software. The static pressure is higher at the resin inlet position compared to the resin outlet position. Maximum pressure was observed at the center area across the inlet and outlet transverse direction. The simulation results are in good agreement with the analytical approach. Mold filling time is higher in thick laminates compared to thin laminates. The average part thickness variation increased from the resin inlet to the resin outlet position for 4, 8, and 12 layer reflectors.

DATA AVAILABILITY STATEMENT

The data that support the findings of this study are available from the corresponding author upon reasonable request.

ORCID

Tushar Gajjar https://orcid.org/0000-0001-9260-9662
Dhaval B. Shah https://orcid.org/0000-0001-6800-5236
Shashikant J. Joshi https://orcid.org/0000-0002-1322-448X
Kaushik M. Patel https://orcid.org/0000-0001-8758-1239

REFERENCES

[1] S. K. Mazumdar, *Composites Manufacturing Materials, Product, and Process Engineering*, CRC Press, **2001**.
[2] I. M. Daniel, O. Ishai, *Engineering mechanics of composite materials*, 2nd ed., Oxford University Press, New York **2006**.
[3] A. K. Kaw, *Mechanics of Composite Materials*, LLC. CRC Press, Taylor & Francis Group **2006**.
[4] R. J. Johnson, R. Pitchumani, *Compos. Sci. Technol.* **2007**, *67* (3–4), 669.
[5] R. J. Johnson, R. Pitchumani, *Compos. Part A: Appl. Sci. Manuf.* **2006**, *37*(10), 1815. https://doi.org/10.1016/j.compositesa.2005.09.007.
[6] R. J. Johnson, R. Pitchumani, *Compos. Sci. Technol.* **2003**, *63* (15), 2201. https://doi.org/10.1016/S0266-3538(03)00179-9.
[7] R. Chen, C. Dong, Z. Liang, C. Zhang, B. Wang, *Polym. Compos.* **2004**, *25*(2), 146. https://doi.org/10.1002/pc.20012.
[8] M. Grujicic, K. M. Chittajallu, W. Shawn, *Appl. Surf. Sci.* **2005**, *245*(1–4), 51. https://doi.org/10.1016/j.apsusc.2004.09.123.
[9] D. Heider, P. Simacek, A. Dominauskas, H. Deffor, S. Advani, J. W. Gillespie Jr.., *Compos. Part A: Appl. Sci. Manuf.* **2007**, *38* (2), 525. https://doi.org/10.1016/j.compositesa.2006.02.016.
[10] N. Kuentzer, P. Simacek, S. G. Advani, S. Walsh, *Compos. Part A: Appl. Sci. Manuf.* **2007**, *38*(3), 802. https://doi.org/10.1016/j.compositesa.2006.08.005.
[11] Song, X. (**2003**). Vacuum assisted resin transfer molding (VARTM): model development and verification (Doctoral dissertation, Virginia Tech).
[12] Y. J. Lee, Y. T. Jhan, C. H. Chung, Y. Hsu, *Engineering* **2011**, *3* (07), 691. https://doi.org/10.4236/eng.2011.37082.
[13] D. Bender, J. Schuster, D. Heider, *Compos. Sci. Technol.* **2006**, *66*(13), 2265. https://doi.org/10.1016/j.compscitech.2005.12.008.
[14] J. M. Bayldon, I. M. Daniel, *Compos. Part A: Appl. Sci. Manuf.* **2009**, *40*(8), 1044. https://doi.org/10.1016/j.compositesa.2009.04.008.
[15] Y. Rachmadini, V. B. C. Tan, T. E. Tay, *J. Reinf. Plast. Compos.* **2010**, *29*(18), 2782. https://doi.org/10.1177/0731684409359103.
[16] J. Dai, D. Pellaton, H. T. Hahn, *Polym. Compos.* **2003**, *24*(6), 672. https://doi.org/10.1002/pc.10061.
[17] J. A. Acheson, P. Simacek, S. G. Advani, *Compos. Part A: Appl. Sci. Manuf.* **2004**, *35*(2), 159. https://doi.org/10.1016/j.compositesa.2003.02.001.
[18] B. Markicevic, D. Heider, S. G. Advani, S. Walsh, *Compos. Part A: Appl. Sci. Manuf.* **2005**, *36*(6), 851. https://doi.org/10.1016/j.compositesa.2004.09.002.

[19] D. B. Shah, K. M. Patel, A. I. Patel, V. Pariyal, S. J. Joshi, *Compos. Part A: Appl. Sci. Manuf.* **2018**, *115*, 134. https://doi.org/10.1016/j.compositesa.2018.09.017.
[20] T. Gajjar, D. Shah, S. Joshi, K. M. Patel, *Curved Layered Struct.* **2019**, *6*(1), 169. https://doi.org/10.1515/cls-2019-0014.
[21] S. Y. Kim, W. J. Choi, S. Y. Park, *Int. J. Adv. Manuf. Technol.* **2007**, *32*(5–6), 445. https://doi.org/10.1007/s00170-005-0355-8.
[22] D. Modi, M. Johnson, A. Long, C. Rudd, *Compos. Sci. Technol.* **2009**, *69*(9), 1458. https://doi.org/10.1016/j.compscitech.2008.05.026.
[23] M. K. Kang, W. I. Lee, H. T. Hahn, *Compos. - Part A: Appl. Sci. Manuf.* **2001**, *32*(11), 1553. https://doi.org/10.1016/S1359-835X.
[24] A. Hammami, B. R. Gebart, *Polym. Compos.* **2000**, *21*(1), 28.
[25] C. J. Dong, *Compos. Part A: Appl. Sci. Manuf.* **2006**, *37*(9), 1316. https://doi.org/10.1016/j.compositesa.2005.08.012.
[26] J. Vilà, C. González, J. LLorca, *J. Compos. Mater.* **2017**, *51*(5), 687. https://doi.org/10.1177/0021998316649783.
[27] C. Arulappan, A. Duraisamy, D. Adhikari, S. Gururaja, *J. Reinf. Plast. Compos.* **2015**, *34*(1), 3. https://doi.org/10.1177/0731684414560220.
[28] C. D. Williams, S. M. Grove, J. Summerscales, *Compos. Part A: Appl. Sci. Manuf.* **1998**, *29*(1–2), 111. https://doi.org/10.1016/S1359-835X(97)00038-9.
[29] B. Yenilmez, M. Senan, E. M. Sozer, *Compos. Sci. Technol.* **2009**, *69*(11–12), 1710. https://doi.org/10.1016/j.compscitech.2008.05.009.
[30] Q. Govignon, S. Bickerton, S. Kelly, *J. Compos. Mater.* **2012**, *47*(12), 1479. https://doi.org/10.1177/0021998312448500.
[31] F. Robitaille, R. Gauvin, *Polym. Compos.* **1998**, *19*(2), 198. https://doi.org/10.1002/pc.10091.
[32] D. Yuexin, T. Zhaoyuan, Z. Yan, S. Jing, *Chinese J. Aeronautics* **2008**, *21*(4), 370. https://doi.org/10.1016/S1000-9361(08)60048-5.
[33] A. Hammami, *Polym. Compos.* **2001**, *22*(3), 337. https://doi.org/10.1002/pc.10542.
[34] N. C. Correia, F. Robitaille, A. C. Long, C. D. Rudd, P. Simacek, S. G. Advani, *Compos. Part A: Appl. Sci. Manuf.* **2005**, *36*(12), 1645. https://doi.org/10.1016/j.compositesa.2005.03.019.
[35] T. Gajjar, D. B. Shah, S. J. Joshi, K. M. Patel, *Mater. Today: Proc.* **2020**, *21*, 1244. https://doi.org/10.1016/j.matpr.2020.01.112.
[36] K. Saleh, O. Abdelaziz, V. Aute, R. Radermacher, S. Azarm, *Appl. Therm. Eng.* **2013**, *61*(2), 817. https://doi.org/10.1016/j.applthermaleng.2012.06.007.

How to cite this article: Gajjar T, Shah DB, Joshi SJ, Patel KM. Experimental investigations on process parameters for manufacturing of antenna reflectors using vacuum infusion process. *SPE Polymers*. 2021;2:19–27. https://doi.org/10.1002/pls2.10026